SLAC-PUB-2059
LBL-7243
December 1977
(T/E)

ANOMALOUS e^+e^- AND $\mu^+\mu^-$ EVENTS PRODUCED IN e^+e^- ANNIHILATION*

F. B. Heile, M. L. Perl, G. S. Abrams, M. S. Alam, A. M. Boyarski, M. Breidenbach, J. Dorfan, G. J. Feldman, G. Goldhaber, G. Hanson, J. A. Jaros, J. A. Kadyk, D. Lüke,** R. J. Madaras, Ann E. Nelson, J. M. Paterson, I. Peruzzi,† M. Piccolo,† T. Pun, P. Rapidis, J. E. Wiss

Stanford Linear Accelerator Center, Stanford University, Stanford, California 94305

and

Lawrence Berkeley Laboratory and Department of Physics University of California, Berkeley, California 94720

and

G. Grammer, Jr.

Physics Department, University of Illinois Urbana, Illinois 61801

ABSTRACT

We have observed events of the form $e^+ + e^- \to e^+ + e^-$ and $e^+ + e^- \to \mu^+ + \mu^-$ in which there are no other detected particles and there is substantial missing energy; and which cannot be explained by conventional electromagnetic interactions. We show that these events can be explained as the decay products from the pair production, $e^+ + e^- \to \tau^+ + \tau^-$, of a new charged lepton, $\tau^\pm$, of mass $1.90 \pm .10$ GeV/c^2. Some properties of these events are presented. In particular, this production cross section is inconsistent with the τ being an electron-related paralepton.

(Submitted to Nuclear Physics)

*Work supported by the Department of Energy.

**Fellow of Deutsche Forschungsgemeinschaft.

†Permanent address: Laboratori Nazionali, Frascati, Rome, Italy.

I. INTRODUCTION

In the past two years substantial evidence has been found [1,2,3] for the existence of a new charged particle called the $\tau^{\pm}$. This particle has a mass [4,5] of 1.90 ± .10 GeV/c; decays predominantly through the weak interactions, and all its known properties are consistent with being a lepton. That is, the $\tau^{\pm}$ appears to be a point particle having no strong interactions, but having electrodynamic and weak interactions.

Part of the evidence for the τ's existence consists of events of the form

$$e^+ + e^- \rightarrow e^{\pm} + \mu^{\mp} + \text{missing energy} \qquad (1)$$

in which no other charged or neutral particles are detected. The only simple explanation [1,4,5] for these events, called eμ events hereafter, is that they come from the production and decay sequence

$$\begin{array}{ccccc} e^+ + e^- & \rightarrow & \tau^+ & + & \tau^- \\ & & \downarrow & & \downarrow \\ & & \bar{\nu}_\tau e^+ \nu_e & & \nu_\tau \mu^- \bar{\nu}_\mu \end{array}$$

or the charged conjugate reaction. These leptonic decays of the τ and the nature of the assumed associated neutrinos, ν_τ, are discussed in sec. II. Since the τ^+ and τ^- decays are independent, if this explanation of the eμ events is correct, the following reactions must also occur:

$$\begin{array}{ccccc} e^+ + e^- & \rightarrow & \tau^+ & + & \tau^- \\ & & \downarrow & & \downarrow \\ & & \bar{\nu}_\tau e^+ \nu_e & & \nu_\tau e^- \bar{\nu}_e \end{array} \qquad (3)$$

$$\begin{array}{ccccc} e^+ + e^- & \rightarrow & \tau^+ & + & \tau^- \\ & & \downarrow & & \downarrow \\ & & \bar{\nu}_\tau \mu^+ \nu_\mu & & \nu_\tau \mu^- \bar{\nu}_\mu \end{array} \qquad (4)$$

Therefore ee and μμ events,

$$e^+ + e^- \to e^+ + e^- + \text{missing energy} \qquad (5a)$$

$$e^+ + e^- \to \mu^+ + \mu^- + \text{missing energy} \ , \qquad (5b)$$

which are analogous to the eμ events must also occur. Indeed on much more general grounds such ee and μμ events must occur, <u>regardless</u> of the nature of the τ, if we simply assume that:

1. the eμ events are real;
2. the e and μ come from the decays of different particles called τ's;
3. the τ's are pair produced;
4. the decays of the $\tau^+\tau^-$ pair are independent of each other.

Therefore it is crucial that such ee and μμ events exist if the new particle explanation of the eμ events is correct. This paper reports:

1. that such ee and μμ events have been found;
2. that their production cross section is consistent with the production cross section of the eμ events if the τ is <u>not</u> a paralepton; and
3. that their properties are consistent with the properties of the eμ events.

These results are based on data acquired using the SLAC-LBL Magnetic Detector at the Stanford Linear Accelerator Center's SPEAR e^+e^- Colliding Beams Facility.

The study of these ee and μμ events is much more difficult than the study of the eμ events because there are purely electromagnetic processes with relatively large cross sections that lead to events of the form of the reactions in eq. (5). For example, the two-virtual-photon processes [6]

$$e^+ + e^- \to e^+ + e^- + e^+ + e^- \qquad (6)$$

$$e^+ + e^- \to \mu^+ + \mu^- + e^+ + e^-$$

can contaminate the reactions in eq. (5) if the second e^+e^- pair is not detected. Such backgrounds are discussed in sec. V.

The apparatus is described in sec. III and the data analysis is presented in sec. IV. The results and conclusions are given in sec. VI.

II. THEORY

The body of theoretical work on leptons, on their relations to quarks, and on gauge theories has grown rapidly in the past few years. Refs. [7-9] provide some introduction to these general theoretical questions concerning leptons. However in this section we shall present only a few simple ideas related to our immediate interest, namely that the ee and μμ events come from a charged heavy lepton whose dominant decay modes are thru the weak interactions. Hence we consider three types of leptons in which the electromagnetic decay modes are forbidden or strongly suppressed.

A. Sequential Heavy Leptons

It is possible that the electron and muons are the smallest mass members of a sequence of charged leptons each having a unique lepton number and a unique associated neutrino:

$$\begin{array}{ll} e^{\pm} & \nu_e,\ \bar{\nu}_e \\ \mu^{\pm} & \nu_\mu,\ \nu_\mu \\ \tau^{\pm} & \nu_\tau,\ \bar{\nu}_\tau \\ \cdot & \cdot \\ \cdot & \cdot \\ \cdot & \cdot \end{array} \qquad (7)$$

The consequence of the unique lepton numbers and complete lepton number conservation is that the electromagnetic decays

$$\tau^- \not\to e^- + \gamma, \quad \tau^- \not\to \mu^- + \gamma \qquad (8)$$

are forbidden and all decays are thru the weak interactions. The purely leptonic decays are then

$$\begin{aligned} \tau^- &\to \nu_\tau + e^- + \bar{\nu}_e \\ \tau &\to \nu_\tau + \mu^- + \bar{\nu}_\mu \end{aligned} \tag{9}$$

Depending on the mass of the τ, m_τ, there may also be hadronic decay modes such as

$$\begin{aligned} \tau^- &\to \nu_\tau + \pi^- \\ \tau^- &\to \nu_\tau + \pi^- + \pi^+ + \pi^- \end{aligned} \tag{10}$$

Although we shall not use it explicitly in this paper, we note that by using conventional weak interaction theory and some measurements from known weak interactions the decay widths and lifetimes of the sequential heavy lepton can be calculated. Table I gives the relative decay rates for a 1.9 GeV/c^2 τ using V-A coupling and $m_{\nu_\tau} = 0.0$ (m_{ν_τ} is the mass of the ν_τ). This yields a lifetime of 2.7×10^{-13} sec [5,10,11].

B. Paraleptons

A paralepton [12], following the notation of Llewellyn Smith [7], has the lepton number of the oppositely charged e or μ. (We formerly called these gauge theory leptons.) Explicitly the E^+ has the lepton number of the e^- with leptonic decay modes

$$E^+ \to e^+ + \nu_e + \nu_e \tag{11a}$$

$$E^- \to e^- + \bar{\nu}_e + \bar{\nu}_e \tag{11b}$$

$$E^+ \to \mu^+ + \nu_\mu + \nu_e \tag{12a}$$

$$E^- \to \mu^- \to \bar{\nu}_\mu + \bar{\nu}_e \tag{12b}$$

and hadronic decay modes

$$E^+ \to \nu_e + \text{hadrons}, \quad E^- \to \bar{\nu}_e + \text{hadrons} \tag{13}$$

Clearly the electromagnetic decay modes are forbidden. A muon associated paralepton, $M^{\pm}$, can also be defined, but the lower limit on its mass [13] set by muon neutrino experiments eliminates it from consideration here.

C. Ortholeptons [7]

Such charged heavy leptons have the same lepton number as the same charge e or μ. We define the e^{*-} to have the lepton number of the e^- and the μ^{*-} to have the lepton number of the μ^-. We also call these particles excited electrons or muons. We expect that their dominant decay will be electromagnetic

$$e^{*\pm} \to e^{\pm} + \gamma \ , \ \mu^{*\pm} \to \mu^{\pm} + \gamma \tag{14}$$

and so such particles would not be of interest here. However as discussed by Low [14] the coupling at the $e^*e\gamma$ and $\mu^*\mu\gamma$ vertices must be of the form

$$(e/M)\bar{\psi}_{e^*}\sigma_{\mu\nu}\psi_e f^{\mu\nu} \tag{15}$$

where M is an arbitrary mass. By making M very large the electromagnetic decays can be suppressed and the weak interaction decays allowed to be dominant.

D. Comparison of Leptonic Decay Rates

If all three types of leptons are assigned V-A coupling and all neutrino masses = 0, for sequential leptons and ortholeptons

$$\frac{\Gamma(\tau^- \to \nu_\tau e^- \bar{\nu}_e)}{\Gamma(\tau^- \to \nu_\tau \mu^- \bar{\nu}_\mu)} = 1 \tag{15a}$$

where Γ is the decay width to the indicated mode. But for paraleptons with V-A coupling and all left-handed neutrinos

$$\frac{\Gamma(E^- \to e^- + \bar{\nu}_e + \bar{\nu}_e)}{\Gamma(E^- \to \mu^- + \bar{\nu}_\mu + \bar{\nu}_e)} = 2 \tag{15b}$$

because there is constructive interference of the two diagrams which give the e^- decay mode [15]. (For further discussion see sec. VI.C.)

E. Production Cross Section

We limit our considerations to the τ being a spin 1/2, Dirac point particle. Then the total production cross section thru one-photon exchange, fig. 1, is

$$\sigma_{\tau^+\tau^-} = \frac{2\pi\alpha^2\beta(3 - \beta^2)}{3s} \tag{16}$$

Here βc is the velocity of the τ and α is the fine structure constant.

III. APPARATUS AND EXPERIMENTAL METHOD

A. SPEAR e^+e^- Colliding Beams Facility

In the SPEAR e^+e^- Colliding Beams Facility, fig. 2, the e^+ and e^- have equal and opposite momenta. Hence the total momentum of an e^+e^- collision is zero and the total energy is

$$E_{c.m.} = 2E_b$$

where E_b is the energy in each beam. We also use $s = E^2_{c.m.}$. SPEAR operates in the energy range of $2 \lesssim E_{c.m.} \lesssim 8$ GeV. The rate at which events are produced from a reaction having a cross section σ is given by

$$\text{rate(events/sec)} = \sigma(\text{cm}^2)L(\text{cm}^{-2}\text{sec}^{-1}) \tag{17}$$

L is called the luminosity. In SPEAR there is just one bunch of electrons and one bunch of positrons moving in opposite directions. Hence the luminosity is given by

$$L = N^2 f/A \tag{18}$$

where N is the number of e^+ or e^- in a bunch, f is the number of bunch collisions per second per interaction region, and A is the cross sectional area of a bunch in cm^2. The instantaneous luminosity at SPEAR at the beginning of a fill is given approximately by $(E_b/1.8)^4 10^{30}\text{cm}^{-2}\text{sec}^{-1}$ for $E_b \lesssim 3$ GeV, and is about $10^{31}\text{cm}^{-2}\text{sec}^{-1}$ for $E_b > 3$ GeV.

This experiment operated in the west pit interaction area of SPEAR (fig. 2).

B. Detector

A drawing of the detector is shown in fig. 3. The magnetic field is provided by a solenoidal coil 3.6 m long and 3.3 m in diameter. The field of approximately 4 kG is longitudinal to the beam axis and is uniform to about ±2%.

We will start at the interaction region and describe in turn each element through which a produced particle passes. The beam pipe has a mean radius of 8 cm and is made of .15 mm thick corrugated stainless steel. The average effective thickness, due to the corrugations, is .20 mm.

Around the beam pipe are four semi-cylindrical scintillators forming two nesting cylinders at 11 and 13 cm radii. These counters are each 7 mm thick and 36 cm long. They are part of the trigger and serve primarily to reduce triggers from cosmic rays.

There are two cylindrical proportional chambers around the beam pipe at 17 and 22 cm radii. Each consists of 512 sense wires parallel to the beam axis and cathode strips perpendicular to the beam axis. These chambers were installed in January 1975. They have no direct effect on the analysis of data presented in this paper.

The main tracking elements of the detector are four modules of concentric cylindrical magnetostrictive spark chambers at radii of 66, 91, 111 and 135 cm. Each module consists of four cylinders of wires with the wires set at +2°, -2°, +4° and -4° with respect to the beam axis. The tracking algorithms require sparks in three of the four modules and thus the angular acceptance is normally defined by the 2.68 m length of the third chamber. Neglecting the finite length of the interactions regions and the curvature of tracks in the magnetic field, these chambers track particles over $.70 \times 4\pi$ sr solid angle. The rms momentum resolution for a 1 GeV/c track is about 15 MeV/c. Because of the high degree of redundancy (three out of four modules, two out of four wires per module required) these chambers are highly efficient in tracking particles. The inefficiency has been estimated at 1% per track

or less. The structural support for the chambers consists of six 6 mm wall, 5 cm diameter, aluminum posts at a radius of 79 cm, and a 1.3 cm thick aluminum cylinder at a radius of 1.49 m. These support posts can be major sources of multiple scattering; for this reason the analysis programs normally require that at least two particles in each event do not pass through a support post so that a good vertex for the event can be found. These posts subtend about 6% of the solid angle so this requirement reduces the effective solid angle of the detector somewhat. The data has been corrected for this.

Immediately beyond the aluminum cylinder supporting the spark chambers is a cylindrical array of 48 2.5 cm thick plastic scintillator trigger counters. They are 2.61 m long and are viewed by 5 cm photomultiplier tubes from both ends. They are part of the trigger and provide time-of-flight information with an rms resolution of about 0.5 ns. This is sufficient to separate pions from kaons up to a momentum of 600 MeV/c and kaons from protons up to a momentum of 1100 MeV/c. The solid angle subtended by these counters is $.65 \times 4\pi$ sr.

Next a particle will pass through the 9 cm aluminum solenoid coil and enter a cylindrical array of 24 lead-plastic scintillator shower counters. The 3.10 m long counters are made of five layers, each layer containing 6.4 mm of lead and 6.4 mm of scintillator. The counters are viewed from each end by a 13 cm photomultiplier tube. They are part of the trigger and have the primary function of discriminating between electrons and hadrons. They also have been used to a limited extent to detect photons.

Beyond the shower counters are a 20 cm thick iron flux return and one or two planar magnetostrictive wire spark chambers to detect muons.

The flux return is an adequate hadron filter for our purposes [16].

C. Trigger

The trigger rate of the magnetic detector is limited to a few triggers per second by the time required to recharge the spark chamber pulsing system. To achieve this low a trigger rate it has been found necessary to require a pipe counter and two sets of trigger counters with associated shower counters to fire. The shower counters are set to fire on minimum ionizing particles. No special trigger was used for the ee, μμ, or eμ events; they were simply acquired as part of the general data acquisition.

D. Data Acquisition

Data were acquired over a three year period ending in 1976. The integrated luminosity upon which this paper is based is

$$\int L dt \approx 16 \text{ pb}^{-1} = 1.6 \times 10^{37} \text{ cm}^{-2}$$

The $E_{c.m.}$ range was 4.0 to 7.8 GeV. Since the data were acquired while the experiment was run for other purposes the data is spread unevenly over the $E_{c.m.}$ range. The main data blocks are

$$E_{c.m.} = 3.9 \text{ to } 4.6 \text{ GeV}, \int L dt = 3.7 \text{ pb}^{-1}$$

$$E_{c.m.} = 4.8 \text{ GeV}, \qquad \int L dt = .9 \text{ pb}^{-1}$$

$$E_{c.m.} = 5.8 \text{ to } 7.8 \text{ GeV}, \int L dt = 10.8 \text{ pb}^{-1}$$

E. Selection of Electrons

The corrected shower counter pulse height, H_c, is defined in units such that for an electron of momentum p

$$\langle H_c(p) \rangle \approx 100\ p \tag{19}$$

where p is in GeV/c. We defined as electrons all particles with

$$H_c(p) > 50 \tag{20a}$$

and

$$p > 0.65 \text{ GeV/c} \tag{20b}$$

We used this fixed lower limit rather than a p dependent limit for three reasons:

a. The pulse height distribution for a fixed p is rather broad:

$$\sigma_{H_c}/H_c \sim .6/\sqrt{p} \quad , \quad p \text{ in GeV/c} \tag{21}$$

b. During the three years of data acquisition various changes were made in the shower counter operating conditions and some degeneration of the scintillator surface in the counters may have occurred. Hence the ratio of the corrected pulse height H_c to the raw pulse height changed with time and several recalibrations of the ratio were made to preserve, eq. (19). These recalibrations used collinear e^+e^- events produced by Bhabha scattering. Nevertheless eq. (19) could not be maintained precisely.

c. Equation (19a) is only approximate, there are nonlinearities in the relations of $H_c(p)$ to p below 1 GeV/c and above 2 or 2.5 GeV/c. For these reasons a fixed lower limit in $H_c(p)$ was easier to use, and losses and corrections easier to evaluate.

The lower limit on p of 0.65 GeV/c was used to reduce the loss of electrons whose H_c was below 50 (see sec. IV.D).

F. Selection of Muons

Muons are sought by looking for sparks in the muon detector chambers (fig. 3) accessible to a particle. Accessible means that the particle had the proper angle and sufficient momentum to reach that chamber. Since a muon will multiple scatter in the iron and other material, we define d_μ as the measured distance between a muon produced spark in a muon chamber and the position of the projected muon track in that

chamber. We define σ_μ as one standard deviation due to the multiple scattering expected in that distance, and we define the ratio

$$D_\mu = d_\mu/\sigma_\mu \tag{22}$$

Muons were then defined by:

$$\begin{aligned} &\text{spark with } |D_\mu| < 4 \\ &p > 0.65 \text{ GeV/c} \\ &H_c < 50 \end{aligned} \tag{23}$$

We note that an e is defined first, hence if $H_c > 50$ a particle is called an e even if $|D_\mu| < 4$.

G. Event Selection

We selected all e^+e^-, $\mu^+\mu^-$ and for comparison purposes $e^{\mp}\mu^{\pm}$ events with the following properties:

1. There are two and only two charged particles detected.
2. Each particle is an e or a μ as defined in eqs. (20) and (23), in particular $p_1 > 0.65$ GeV/c and $p_2 > 0.65$ GeV/c.
3. The particles have opposite electric charge.
4. There are no photons detected. The efficiency for photon detection is close to 100% for photon energies above 200 MeV but falls to zero when the photon energy is 20 or 30 MeV.
5. The coplanarity angle, θ_{copl}, is greater than 20° where

$$\cos\theta_{copl} = -(\underset{\sim}{n}_1 \times \underset{\sim}{n}_+)\cdot(\underset{\sim}{n}_2 \times \underset{\sim}{n}_+)/(|\underset{\sim}{n}_1 \times \underset{\sim}{n}_+|\cdot|\underset{\sim}{n}_2 \times \underset{\sim}{n}_+|) \tag{24}$$

Here $\underset{\sim}{n}_1$, $\underset{\sim}{n}_2$ and $\underset{\sim}{n}_+$ are unit vectors in the direction of motion of particle 1, particle 2 and the incident e^+ beam respectively. This cut eliminates the very large number of coplanar $e^+e^- \to e^+e^-$ and $e^+e^- \to \mu^+\mu^-$ events.

6. The missing mass squared, m_m^2, is greater than 2.0 $(GeV/c^2)^2$. Here

$$m_m^2 = (E_{c.m.} - E_1 - E_2)^2 - (\underset{\sim}{p}_1 + \underset{\sim}{p}_2)^2 \tag{25}$$

where E_i, p_i are the energy and three-momentum of particle i.

7. An angular cut of $|\cos \theta_i| \leq 0.6$ is also used, where θ_i is the angle between particle i and the e^+ beam direction. This cut was more severe than was used in our other $e^{\pm}\mu^{\mp}$ studies and reduces the number of events somewhat. It was made in order to provide a very well defined angular acceptance for electrodynamic process background calculation.

H. Background Event Selection

For background studies we collected all other 2-prong events in which all criteria of the previous section except 2. were met and in which both particles had $p > 0.65$ GeV/c. Such events contain one or two particles which are neither e's nor μ's. We call these particles

h (for hadron) if a muon chamber was accessible
x (for hadron or muon) if a muon chamber was not accessible (26)

For most of the experiment we did not have complete coverage of muon chambers, but we always had complete coverage by the electron defining shower counters. Hence there can be hadron-muon ambiguities but there are no hadron-electron ambiguities.

IV. DATA ANALYSIS

A. Uncorrected Data

Table II gives the numbers of events in 5 $E_{c.m.}$ ranges for the uncorrected data. If there were no anomalous sources of leptons, no hadron decays to leptons and no misidentification of particles we would see only ee, μμ and hh events. However we know that the τ produces eμ events. Therefore more generally we should see ee, μμ, eμ and hh events. We obviously see other types of events due partly to particle misidentification and also due perhaps to other decay modes of the τ (sec. II.A). Our next task is to consider this misidentification problem.

B. Misidentification Probabilities

Some e's selected by the cuts in eq. (20) may be hadrons which have interacted in the shower counter giving $H_c > 50$. Other e's may come from $K^{\pm}_{e3}$ decay and hence constitute a background for e's from τ decay. Similarly, some of the μ's will not be muons since a hadron can punch through the iron and simulate a muon. Hence to determine the actual number of ee's, μμ's or eμ's we will have to correct for these and all other possible misidentifications. To do this correction we need to know the probability that a particle that is actually an e, μ, or h will be classified as an e, μ, h or x. We will call this probability $P_{i \to n}$ where i is one of e, μ, or h, and n is one of e, μ, h or x.

The two largest and most important misidentification probabilities are $P_{h \to e}$ and $P_{h \to \mu}$. These were determined by assuming that every prong in a three or more pronged event was actually a hadron. Hence by counting how many of these prongs would have been classified as either an e or a μ we arrive at $P_{h \to e}$ and $P_{h \to \mu}$ as the ratio of the numbers

of e's and μ's to the total number of hadrons respectively. This is momentum dependent, and the determination was done in different momentum bins and the results folded with the hadron momentum spectrum observed in our two prong events to arrive at the probabilities shown in Table III. Note that $P_{h \to e}$ and $P_{h \to \mu}$ are actually upper bounds since they include not only the effects of hadronic decay, interaction, and punch through, but also include any direct lepton production (from charmed particles or the τ) in the three or more prong events as an event where a hadron is misidentified. Therefore we are overestimating $P_{h \to e}$ and $P_{h \to \mu}$.

Another fairly large misidentification probability is $P_{e \to h}$ which is caused by a fluctuation of the electron's shower pulse height below our cut. Obviously this is momentum dependent since a low momentum electron will have a much higher chance of being misidentified as a hadron. This probability was calculated by using radiative Bhabha events as a source of known electrons at different energies. Then in each momentum bin the ratio of electrons with showers below the cut to all electrons in that bin gives $P_{e \to h}$ for that momentum. This was folded with the observed momentum distribution of electrons in our sample to give the actual $P_{e \to h}$ shown in Table III.

At various times some of the muon chambers were removed, and in addition there are gaps between the muon chambers where the muon detection efficiency decreases, therefore the category x consists of tracks with $H_c < 50$ that are heading for these areas. Thus $P_{\mu \to x}$ and $P_{h \to x}$ are equal to the fraction of the solid angle without muon detection. Also

$$P_{e \to x} = P_{e \to h} P_{h \to x} \tag{27}$$

$$P_{e \to \mu} = .01\, P_{e \to h}(1 - P_{h \to x}) \tag{28}$$

where the .01 in eq. (28) is the probability that an e will give a spark with $|D_\mu| < 4$ in a muon chamber. Finally $P_{\mu \to h}$ is given by our muon chamber inefficiency as measured by collinear muons and we estimate .001 for $P_{\mu \to e}$.

C. Correction of Data for Misidentification--General

Using the P's in Table III we must now correct the raw data in Table II. An exact procedure requires knowledge of the decay modes of the τ, and perhaps other new particles, which can produce eh and μh events. For example, the production of a $\tau^+\tau^-$ pair can yield such events if one τ decays into an e or μ and the other τ decays semi-leptonically into a charged hadron, a neutrino, and either no photons or no detected photons.

However, at present we do not know what relative numbers of real eh and μh events to expect. Therefore we have used three different methods to correct the raw data in Table II. These methods are:

Method I: We assume that the $\tau^+\tau^-$ pair produces only ee, $\mu\mu$, and eμ events, and perhaps hh events. We assume that all backgrounds are hh events. Hence we assume there are no actual eh or μh events. This method uses a χ^2 minimization procedure.

Method II: We allow in addition to the actual ee, $\mu\mu$, eh and hh events of Method I, actual eh and μh events. These might come from $\tau^+\tau^-$ decays or be background events. However, we assume on the basis of μ-e universally that the number of actual eh events equals the number of actual μh events. This assumption is used to reduce the magnitude of the errors resulting from the minimization procedure which we use.

Method III: Here we allow actual ee, eμ, hh, eh, and μh events with no restriction on the relation of the number of eh to the number of μh events. This method uses a matrix inversion procedure so that it also tests for the number of actual ex, μx, hx and xx events--numbers which by the definition of x should be consistent with zero within these errors.

D. Event Misidentification Correction Using Method I

We assume that only real ee, μμ, eμ, and hh events exist.

We define

$N_0(ij)$ = the number of observed events of type i,j

$N_a(nm)$ = the actual number of events of type n,m

$N_p(ij)$ = the predicted number of events of the type i,j derived from $P_{i \to h}$ and $N_a(nm)$

where i,j = e, μ, h, x and n,m = e, μ, h.

We then minimize

$$\chi^2 = \sum_{i,j} \left[(N_0(ij) - N_p(ij) \right]^2 / N_0(ij) \tag{29}$$

with respect to $N_a(nm)$. For example if only $N_a(ee)$, $N_a(\mu\mu)$ and $N_a(hh)$ are allowed to be non-zero

$$N_p(e\mu) = 2N_a(ee)P_{e \to e}P_{e \to \mu} + 2N_a(\mu\mu)P_{e \to \mu}P_{\mu \to \mu} + 2N_a(hh)P_{h \to e}P_{h \to \mu} \tag{30}$$

If we assume that the only actual events allowed are ee's, μμ's, and hh's, we find that we cannot obtain a satisfactory minimum χ^2. In fact the category of observed events that is the most inconsistent with the predicted events are the eμ's, with the eμ's observed being consistently about 4 to 5 standard deviations above the eμ's predicted. This of

course agrees with the conclusions of our previous papers on eμ events [1]. Therefore we see that we must expand our class of allowed actual events to include ee's, μμ's, hh's, and eμ's. When this is done we find that we do get reasonable χ^2 and that all ten classes of observed events agree with the predicted events. The results are shown in Table IV.

E. Event Misidentification Correction Using Method II

This method uses the same procedure as Method I except that the allowed actual event types are ee, μμ, eμ, hh, eh and μh and we require $N_a(eh) = N_a(\mu h)$.

F. Event Misidentification Correction Using Method III

We define two 1 x 10 column matrices: D which gives the number of observed events, and A which gives the number of actual events. Specifically:

$$D = \begin{matrix} N_0(ee) \\ N_0(e\mu) \\ N_0(eh) \\ N_0(ex) \\ N_0(\mu\mu) \\ N_0(\mu h) \\ N_0(\mu x) \\ N_0(hh) \\ N_0(hx) \\ N_0(xx) \end{matrix} \quad ; \qquad A = \begin{matrix} N_a(ee) \\ N_a(e\mu) \\ N_a(eh) \\ N_a(ex) \\ N_a(\mu\mu) \\ N_a(\mu h) \\ N_a(\mu x) \\ N_a(hh) \\ N_a(hx) \\ N_a(xx) \end{matrix} \tag{31a}$$

Then D and A are related by a 10 x 10 matrix M

$$D = MA \tag{31b}$$

where for example the elements of M are given by

$$M_{ee \to e\mu} = 2P_{e \to e}P_{e \to \mu}$$

$$M_{ee \to ee} = P^2_{e \to e} \qquad (32)$$

$$M_{e\mu \to e\mu} = P_{e \to e}P_{\mu \to \mu} + P_{e \to \mu}P_{\mu \to e}$$

We then invert the matrix M to yield

$$A = M^{-1}D \qquad (33)$$

Taking D from Table II and calculating M from Table III, we find A for the five sets of data, Table V. Since there is no constraint on the elements of matrix A, negative numbers may, and do, appear. A pleasing aspect of this method is that all values of $N_a(ex)$, $N_a(\mu x)$, $N_a(hx)$, and $N_a(xx)$ are consistent with zero within their errors. This is as it should be, because x is a designation for an observed particle type, and an actual particle type can only be e, μ or h. The consistency of $N_a(ex)$, $N_a(\mu x)$, $N_a(hx)$ and $N_a(xx)$ with zero means that our misidentification probabilities, $P_{i \to \mu}$, are correct within the statistical errors of this analysis.

G. Correction for Inefficiencies

Before we can subtract the electromagnetic processes background we must correct our events for any detection inefficiencies. The hardware trigger requires that there be two shower counters latched. For a muon track we measure a latching efficiency of 94% whereas for electrons we assume the efficiency is 100%. In the software we impose a time of flight cut which will throw out 1% of our tracks. The software track finding efficiency is 98%. And from a study of very collinear Bhabha and mu-pair events with the momentum of each track very close to the beam energy, we conclude that an electron track has an 8% chance of

having an extra shower counter latching but that a muon has only a 2.5% chance. Since we require that our events have no extra shower counters latched, we must include this as an inefficiency. Now when we multiply all of these together we find that we are 83% efficient for electrons and 83% efficient for muons. Thus on a per event basis we are 69% efficient. This correction applies to the data from all the methods. Next we need to know the backgrounds from purely electrodynamic processes.

V. THE BACKGROUND FROM PURELY ELECTROMAGNETIC PROCESSES

There are two different types of purely electromagnetic processes that can survive our experimental cuts and mimic an anomalous dilepton event. An example of the first type is

$$e^+ + e^- \rightarrow e^+ + e^- + \gamma + \gamma \tag{34}$$

which we call a two real photon process since there are two photons in the final state. An example of the second type is

$$e^+ + e^- \rightarrow e^+ + e^- + \mu^+ + \mu^- \tag{35}$$

which we call a two virtual photon process since there are two virtual photon lines in the Feynman diagram. The cross section for each of these processes is integrated over the following phase space for the two leptons that enter the detector (see secs. III.F and III.G).

$$\begin{aligned} &p_1 > 0.65 && p_2 > 0.65 \text{ GeV} \\ &|\cos(\theta_1)| < 0.6 && |\cos(\theta_2)| < 0.6 \\ &m_m^2 > 2.(\text{GeV}/c^2)^2 && \theta_{\text{copl}} > 20^\circ \end{aligned} \tag{36}$$

In addition cylindrical symmetry about the beam direction is assumed. The phase space permitted for the additional leptons or photons will be discussed in the following sections.

A. Two Virtual Photon Processes

The diagrams for the two virtual photon process are shown in fig. 4 for the case of $e^+e^- \rightarrow e^+e^-\mu^+\mu^-$. The evaluation of these diagrams requires a seven dimensional phase space integration of a complicated matrix element. This was accomplished by the use of a program written by Grammer and Kinoshito [6] which integrates the exact matrix element over our phase space. The initial electron and positron were required to not enter the detector i.e. $|\cos\theta| > 0.6$.

The results of these calculations are shown in Table VI for the case of ee or μμ final states. The cross sections computed by the program are actually equal but radiative corrections have been applied to the ee case. A study of the momentum spectrum of the ee's led to an estimate of approximately a 10% correction per electron track to account for the probability that an electron would radiate to below the 0.65 GeV momentum cut.

This is the lowest order purely electromagnetic process that could give $e^{\pm}\mu^{\mp}$ events. Our calculations and a calculation by Zipse [17] show that this cross section is negligible (less than a picobarn). This is also confirmed by the experimental data [1] since one would expect an equal number of charge = ±2 eμ events as charged = 0 eμ events, whereas the data shows almost no charge = ±2 eμ events.

B. Two Real Photon Process

Typical diagrams for the two real photon process are shown in fig. 5. Because of the much larger number of diagrams in this case compared to the two virtual photon case it is impractical to attempt an exact calculation. The approximation we used is to make an exact calculation for one of the photons and a peaking approximation for the other photon. The constraint that the missing mass squared be greater than 2.0 $(\text{GeV}/c^2)^2$ ensures that there be some lower limit to the energy of the peaking photon thus avoiding infrared problems.

First let us consider the case $e^+e^- \to e^+e^-\gamma\gamma$. The program of Berends, Gastman and Gaemers [18] was used to calculate the exact cross section for $e^+e^- \to e^+e^-\gamma$. With the help of K.J.F. Gaemers the program was modified so that the exact single photon cross section was multiplied by the following factor for the peaking photon:

$$\frac{2\alpha}{\pi} \sum_i \ln\left(\frac{2p_i}{m_e} - 1\right)\left(\ln\frac{\omega_{max}}{\omega_{min}} - \frac{\omega_{max} - \omega_{min}}{2E} + \frac{\omega_{max}^2 - \omega_{min}^2}{4E^2}\right) \qquad (37)$$

The sum is over the initial and final state leptons with p_i the momentum of the lepton. The beam energy is E and ω_{max}, ω_{min} are the maximum and minimum energies of the peaking photon respectively. As we sum over each lepton, ω_{min} is the minimum energy that a photon could have and still produce a missing mass squared greater than $2.0(\text{GeV}/c^2)^2$. For the two initial leptons we set ω_{max} equal to the energy of the extra photon; for the two final leptons we use the minimum of either the extra photon energy or $p_i - p_{min}$. And if at any time ω_{min} is greater than ω_{max}, that term in the sum is set equal to zero. The results we obtained are shown in Table VI.

VI. RESULTS AND DISCUSSION

A. Corrected Numbers of Events

Table VII gives the numbers of events corrected for misidentification using Method I, corrected for triggering inefficiencies, and corrected for the purely electrodynamic backgrounds in Table V. The ee and eμ events are also corrected for electron losses due to radiation by the electron; which result on the average in the number of ee events being multiplied by 1.23 and the number of eμ events being multiplied by 1.11. The number of events and cross sections in Table VII are <u>not</u> corrected for the kinematic cuts:

$$\begin{aligned} &|\cos\theta_1| < 0.6 \quad , \quad |\cos\theta_2| < 0.6 \\ &P_1 > 0.65 \text{ GeV/c} \quad , \quad P_2 > 0.65 \text{ GeV/c} \\ &\theta_{\text{copl}} > 20^\circ \\ &m_m^2 > 2.0(\text{GeV/c})^2 \end{aligned} \tag{37}$$

We shall not correct for these cuts here, but to orient the reader we note that for events coming from $\tau^+\tau^-$ decays these cuts result in a 15 to 20% acceptance.

The cross sections in Table VII are given to allow the reader to compare them directly with the purely electromagnetic contributions in Table VI; remembering that the latter cross sections have already been subtracted to yield the cross sections in Table VII. In future tables, however, we shall only present the numbers of events, since that is all we need to calculate ratios. Incidentally, the observed $\sigma_{e\mu}$ cross sections which appear in Table VII are larger than those which have been published in our papers [1,2] because the latter are

not corrected for any losses or trigger inefficiencies. Also there are statistical differences because the latter cross sections are based on a larger data sample.

The corrected numbers of events using Methods II and III are given in Tables VIII and IX, respectively.

Looking at Tables VII, VIII and IX, we conclude that irrespective of the method:

1. Anomalous ee and μμ events have been found in e^+e^- annihilations.
2. The observed cross sections are of the same order of magnitude as that of the anomalous eμ events. This of course is what we expect from our explanation of the eμ events being produced by the pair production process $e^+e^- \to \tau^+\tau^-$.

In comparing all event numbers in the tables we see that Methods II and III give very similar values for $N_{e\mu}$, N_{ee}, and $N_{\mu\mu}$. But Method I (Table VII) gives about 30% higher values. This is because the setting of $N_{e\mu} = N_{\mu\mu} = 0$ in Method I redistributes these events into the other categories.

B. $N_{ee}/N_{e\mu}$ and $N_{\mu\mu}/N_{e\mu}$ Ratios

Table X lists the $N_{ee}/N_{e\mu}$ and $N_{\mu\mu}/N_{e\mu}$ ratios from the three methods. Before considering these ratios we discuss the systematic errors. Those systematic errors which can equal or exceed the statistical errors have the following sources:

a. The subtraction of backgrounds from misidentification of hadrons as e's or μ's has systematic errors because of our empirical method for finding $P_{h \to e}$ and $P_{h \to \mu}$.

b. The correction for muon losses due to $P_{\mu \to h}$ and $P_{\mu \to x}$ has some uncertainties.

c. The correction for electron losses due to $P_{e \to h}$ and to the loss of e's because they radiate has uncertainties, particularly when the e momentum is near the 0.65 GeV/c cut.

d. There are uncertainties in the calculation of the purely electromagnetic backgrounds, particularly in the calculation of $e^+e^- \to e^+e^-e^+e^-$ and $e^+e^- \to e^+e^-\gamma\gamma$.

Table XI gives the maximum systematic errors in the ratios.

Returning to Table X, we see that all the methods give the same ratios within their statistical errors; therefore it fortunately doesn't matter what set of ratios we use. We say fortunate because we have no sure way to know what method is correct. However for the remaining parts of this paper we shall use Method II's values, on the argument that Method I is too restrictive and that Method III gives the same results as Method II, but with larger errors.

C. Comparison With the Heavy Lepton Hypothesis

We use the experimental values

$$\begin{aligned} N_{ee}/N_{e\mu} &= 0.56 \pm .14 \pm \begin{matrix} .16 \\ .19 \end{matrix} \\ N_{\mu\mu}/N_{e\mu} &= 0.70 \pm .15 \pm .19 \end{aligned} \tag{38}$$

Here the first error is one standard deviation statistical error and the second error is the maximum systematic error (see Table XI).

From eq. (15a) we find that for sequential lepton or an ortho-lepton:

$$N_{ee}/N_{e\mu} = 0.5 \quad , \qquad N_{\mu\mu}/N_{e\mu} = 0.5 \tag{39a}$$

For an e-related paralepton with our kinematic cuts (eqs. (37)) eq. (15b) is slightly changed [19] and we obtain for V-A coupling and all left-handed neutrinos

$$N_{ee}/N_{e\mu} = 0.86 \quad , \qquad N_{\mu\mu}/N_{e\mu} = 0.29 \tag{39b}$$

Comparison of eq. (39) with eq. (38) shows that our results are consistent with eq. (39a) but are inconsistent with eq. (39b). If we use zero systematic errors the probability of the values in eq. (38) fitting eq. (39b) is 6.3×10^{-5}; if we use the maximum systematic errors that probability reduces to 1.1×10^{-2}. Hence our third conclusion is:

3. The τ can be a sequential lepton or ortholepton. It cannot be an E type paralepton with V-A coupling and all left-handed neutrinos from our data. [20]

For a μ-related paralepton, theory demands ,

$$N_{ee}/N_{e\mu} = 0.29 \qquad N_{\mu\mu}/N_{e\mu} = 0.86 \tag{39c}$$

This is inconsistent with the values in eq. (38) but not as inconsistent as is the e-related paralepton hypothesis. However the τ being a μ-related paralepton with normal coupling is already ruled out by muon neutrino experiments (sec. II.B).

D. Comparative Properties of the ee, $\mu\mu$ and $e\mu$ Events

Figure 6 gives the r distribution (formerly called the ρ distribution [1,2]) of the momenta, where

$$r = \frac{p - 0.65}{p_{max} - 0.65} \quad , \quad 0 \leq r \leq 1 \tag{40}$$

is a momentum scaling variable which allows us to combine data with different $E_{c.m.}$ values. These data are not corrected for purely electromagnetic backgrounds (sec. V and Table VI), but they are corrected for hadronic backgrounds. Our limited statistics and r-dependent systematic errors make it unprofitable for us to attempt to quantitatively correct the r distributions for the electromagnetic background

bin by bin. To make a rough comparison we fit the eμ distributions with the r curve expected for a heavy lepton with $m_\tau = 1.9$ GeV/c^2, $m_{\nu_\tau} = 0.0$, and V-A coupling. (The fit is obtained by adjusting the leptonic branching ratio.) The same curve multiplied by 0.5 is then drawn in the ee and μμ distributions. We see that within statistics the ee's and μμ's are higher in every r bin, which is what we expect from the purely electromagnetic background which has not been subtracted. We conclude:

4. The total r distributions for the ee and μμ events can contain the r distribution expected from the τ.

We expect that the purely electromagnetic processes ee → eeee and ee → eeμμ will contribute a peak in the r distribution as r → 0. We see such a peak clearly in all the μμ distributions, in the $E_{c.m.} \geq 4.8$ ee distributions; but not in the $E_{c.m.} < 4.8$ ee distribution. We believe this absence of a peak in the last case is due to insufficient correction for e losses near the 0.65 GeV/c momentum cutoff. The relevant systematic error in Table XI is large enough to allow for this uncorrected loss; but we have not adjusted the e loss correction to give such a peak because that would beg the question.

Figure 7 gives the $\cos\theta_{coll}$ distributions [1,2] where

$$\cos\theta_{coll} = -(\underset{\sim}{p}_1 \cdot \underset{\sim}{p}_2)/(|p_1||p_2|) \qquad (41)$$

Note that when the particles are moving in exactly opposite directions, $\underset{\sim}{p}_1 = -\underset{\sim}{p}_2$, $\theta_{coll} = 0$ and $\cos\theta_{coll} = +1$. As in the r distribution case we do not attempt to correct for the electromagnetic backgrounds. The stepped line is a fit to the eμ $\cos\theta_{coll}$ distribution for a heavy lepton with $m_\tau = 1.9$ GeV/c^2, $m_{\nu_\tau} = 0.0$ and V-A coupling. The stepped lines in the ee and μμ distributions are obtained by multiplying the

$e\mu$ line by 0.5. We conclude:

5. The ee and $\mu\mu$ cos θ_{coll} distributions can contain the cos θ_{coll} distribution expected from the τ. The excess events in the cos $\theta_{coll} > 0.6$ bins are what is expected from the electromagnetic backgrounds $ee \rightarrow eeee$, $ee\mu\mu$, $ee\gamma\gamma$, $\mu\mu\gamma\gamma$.

E. Conclusions

Conclusions 1-5 taken together say that all the data which we have on anomalous ee and $\mu\mu$ events is consistent with the τ being a mass $1.90 \pm .10$ GeV/c^2 charged lepton; and it can be either a sequential lepton or an ortholepton.

VII. ACKNOWLEDGEMENT

We are very grateful to K.J.F. Gaemers for his help with the calculations of the electromagnetic backgrounds. He is writing a separate paper on these calculations. We are also very grateful to P. Lepage for his help with these calculations.

REFERENCES

[1] M. L. Perl et al., Phys. Rev. Lett. 35 (1975), 1489; M. L. Perl et al., Phys. Lett. 63B (1976), 117.

[2] G. J. Feldman et al., Phys. Rev. Lett. 38 (1976), 177.

[3] H. Meyer in Proceedings of the Orbis Scientiae - 1977 (Coral Gables, 1977), to be published.

[4] M. L. Perl in Proceedings of the XII Rencontre de Moriond (Flaine, 1977), edited by Tran Thanh Van, R.M.I.E.M. Orsay.

[5] G. J. Feldman in Proceedings of the 1976 Summer Institute on Particle Physics (SLAC, Stanford, 1976); also issued as SLAC-PUB-1852 (1976).

[6] N. Arteaga-Romero, A. Jaccarini and P. Kessler, C.R. Acad. Sci. B269 (1969), 153, 1129; N. Arteaga-Romero, A. Jaccarini, P. Kessler and J. Parisi, Nuovo Cimento Letters 4 (1970), 933; Phys. Rev. D3 (1971), 1569. V. N. Baier and V. S. Fadin, Nuovo Cimento Letters 1 (1971), 481; Phys. Letters 35B (1971), 156; ZhETF (USSR) 61 (1971), 476; JETP (Sov. Phys.) 34 (1972), 253. V. E. Balakin, V. M. Budnev and I. F. Ginzburg, ZhETF Pisma 11 (1970), 557; JETP Letters (Sov. Phys.) 11 (1970), 388. S. J. Brodsky, T. Kinoshita and H. Terazawa, Phys. Rev. Lett. 25 (1970), 972; Phys. Rev. D4 (1971), 1532. V. M. Budnev, V. L. Chernyak and I. F. Ginzburg, Nucl. Phys. B34 (1971), 470. G. Grammer, Jr., and T. Kinoshita, Nucl. Phys. B80 (1974), 461; H. Terazawa, Rev. Mod. Phys. 45 (1973), 615.

[7] C. H. Llewellyn Smith, Oxford Univ. Preprint 33/76 (1976), submitted to Proc. Royal Soc.

[8] A. Pais, Rockefeller Univ. Report COO-2232B-118 (1977).

[9] H. Fritzsch in Proceedings of the XII Rencontre de Moriond (Flaine, 1977), edited by Tran Thanh Van, R.M.I.E.M. Orsay.

[10] H. B. Thacker and J. J. Sakarai, Phys. Lett. 36B (1971), 103.

[11] Y. S. Tsai, Phys. Rev. D4 (1971), 2821.

[12] J. D. Bjorken and C. H. Llewellyn Smith, Phys. Rev. D7 (1973), 88.

[13] B. C. Barish et al., quoted by D. C. Cundy in Proceedings of the XVII International Conference on High Energy Physics (London, 1974), p. IV-147.

[14] F. E. Low, Phys. Rev. Lett. 14 (1965), 238.

[15] A. Ali and T. C. Yang, Phys. Rev. D14 (1976), 3052.

[16] J. T. Dakin and G. J. Feldman, Nucl. Inst. Meth. 116 (1976), 323.

[17] J. E. Zipse, Ph.D. Thesis entitled "Quantum Electrodynamics with the SPEAR Magnetic Detector" (1975), issued as LBL Report LBL-4281 (1975).

[18] F. A. Berends et al., Nucl. Phys. B57 (1973), 381.

[19] Y. S. Tsai, private communication.

[20] S. P. Rosen (to be published) has discussed the more general case in which a paralepton is not restricted to V-A coupling and all left-handed neutrinos. In some of these more general cases our data does not exclude the τ^- having the same lepton number as the e^+.

TABLE I

Predicted branching ratios for a τ^- sequential charged heavy lepton with a mass 1.9 GeV/c^2, an associated neutrino mass of 0.0, and V-A coupling. The predictions are based on Refs. 10 and 11 as discussed in Ref. 5. The hadron continuum branching ratio assumes a threshold at 1.2 GeV for production of $\bar{u}d$ quark pairs whose final state interaction leads to the hadron continuum.

Decay Mode	Branching Ratio	Number of Charged Particles in Final State
$\nu_\tau e^- \bar{\nu}_e$	.20	1
$\nu_\tau \mu^- \bar{\nu}_\mu$	.20	1
$\nu_\tau \pi^-$	.11	1
$\nu_\tau K^-$	.01	1
$\nu_\tau \rho^-$	.22	1
$\nu_\tau K^{*-}$	.01	1
$\nu_t A_1^-$	.07	1, 3
ν_τ(hadron continuum)$^-$	.18	1, 3, 5

TABLE II

Number of raw events. The data in the fifth column were obtained in the first year of the detector operation. This data will be analyzed separately from the later data in the first four columns because of different operating conditions.

Event Type	E_{cm} Range (GeV)	3.9-4.3	4.3-4.8	4.8-6.8	6.8-7.4	3.9-4.8	All Events
	Data Set	2	2	2	2	1	
ee		9	18	47	70	18	162
eμ		15	10	48	44	26	143
eh		11	12	28	32	18	101
ex		10	13	31	38	9	101
μμ		13	19	30	37	13	112
μh		15	13	21	14	12	75
μx		14	23	36	36	11	120
hh		3	3	7	14	7	34
hx		18	10	18	20	4	70
xx		3	3	6	12	4	28
TOTAL		111	124	272	317	122	946

TABLE III

The misidentification probabilities $P_{a\to b}$ described in the text.

E_{cm} range (GeV)	3.9-4.3	4.3-4.8	4.8-6.8	6.8-7.4	3.9-4.8
Data Set	2	2	2	2	1
$P_{e\to\mu}$	$\sim$.002	$\sim$.002	$\sim$.002	$\sim$.002	$\sim$.002
$P_{e\to h}$	.098	.125	.097	.107	.149
$P_{e\to x}$	.0002	.0003	.0002	.0002	.0002
$P_{\mu\to e}$	.001	.001	.001	.001	.001
$P_{\mu\to h}$	.014	.011	.019	.022	.045
$P_{\mu\to x}$	.30	.30	.30	.30	.14
$P_{h\to e}$	.16	.33	.26	.30	.19
$P_{h\to\mu}$	.14	.14	.14	.15	.18
$P_{h\to x}$	.30	.30	.30	.30	.15

TABLE IV

Number of events corrected for misidentification using Method I, but not corrected for triggering inefficiencies (electromagnetic background) or acceptances. The errors are statistical. In this and all following tables the event numbers are rounded off to the nearest event to simplify the tables but calculations were carried out using an additional significant figure.

	E_{cm} Range (GeV)	3.9-4.3	4.3-4.8	4.8-6.8	6.8-7.4	3.9-4.8
	Data Set	2	2	2	2	1
Event Type						
eμ		29±7	21±7	76±11	59±13	39±8
ee		14±6	25±7	58±10	77±11	26±7
μμ		27±6	42±7	62±10	70±11	24±7
hh		41±11	36±7	76±18	111±20	33±12
Total		111	124	272	317	122

TABLE V

Number of events corrected for misidentification using Method III, but not corrected for triggering inefficiencies, electromagnetic background, or acceptance. The errors are statistical.

	E_{cm} Range (GeV)	3.9-4.3	4.3-4.8	4.8-6.8	6.8-7.4	3.9-4.8
	Data Set	2	2	2	2	1
Event Type						
ee		7±4	16±13	46±13	85±21	19±7
eμ		12±8	-8±11	54±17	69±21	29±9
eh		20±12	13±39	33±33	-31±50	21±15
ex		-4±5	4±9	0±10	12±14	3±4
μμ		19±8	30±11	54±13	80±16	16±6
μh		40±16	49±27	46±26	-23±27	10±12
μx		-9±8	0±11	2±13	0±14	7±5
hh		9±10	19±22	34±22	122±42	16±12
hx		22±14	5±17	10±18	3±22	-2±7
xx		-5±2	-4±2	-7±3	0±4	3±2
Total		111	124	272	317	122

TABLE VI

Calculated purely electromagnetic contributions to the observed e^+e^- and the $\mu^+\mu^-$ cross sections. The cross sections are in pb and are calculated for the kinematic cuts in eq. 35. The particles in the parenthesis in the final state are not observed.

			$e^+e^- \rightarrow$			
Data Set	E_{cm} Range (GeV)	Average E_{cm} (GeV)	$e^+e^-(e^+e^-)$	$\mu^+\mu^-(e^+e^-)$	$e^+e^-(\gamma\gamma)$	$\mu^+\mu^-(\gamma\gamma)$
2	3.9-4.3	4.1	1.5	1.9	3.2	0.25
2	4.3-4.8	4.4	1.9	2.4	3.6	0.30
2	4.8-6.8	6.2	4.4	5.4	4.4	0.36
2	6.8-7.4	7.2	5.8	7.2	4.3	0.35
1	3.9-4.8	4.5	2.0	2.5	3.6	0.30

TABLE VII

Using Method I, the corrected numbers of events $N_{e\mu}$, N_{ee}, $N_{\mu\mu}$, and N_{hh}; their ratios; and the observed cross sections, $\sigma_{e\mu}$, σ_{ee}, and $\sigma_{\mu\mu}$ in pb. The numbers and cross sections are corrected for the purely electromagnetic backgrounds in Table VI and for misidentification losses and triggering efficiencies. They are not corrected for the kinematic cuts in eq. 37. The errors are statistical.

E_{cm} Range (GeV)	3.9-4.3	4.3-4.8	4.8-6.8	6.8-7.4	3.9-4.8	all events
Data Set	2	2	2	2	1	1, 2
Luminosity (pb^{-1})	1.88	1.81	4.49	6.85	1.85	16.88
$N_{e\mu}$	46±11	34±10	121±18	95±21	62±13	358±34
N_{ee}	13±10	33±12	55±18	52±20	34±12	187±33
$N_{\mu\mu}$	35±9	56±10	64±14	49±16	29±9	233±27
N_{hh}	60±16	52±17	111±26	162±30	48±18	433±49
$N_{ee}/N_{e\mu}$	0.29±.22	0.96±.44	0.45±.16	0.55±.24	0.55±.22	0.52±.10
$N_{\mu\mu}/N_{e\mu}$	0.76±.26	1.62±.57	0.53±.14	0.52±.20	0.47±.18	0.65±.10
$\sigma_{e\mu}$	24.7±5.6	18.9±5.8	27.0±4.1	13.8±3.1	33.7±6.9	
σ_{ee}	7.1±5.2	18.1±6.4	12.3±3.9	7.6±2.9	18.5±6.4	
$\sigma_{\mu\mu}$	18.7±4.8	30.7±5.6	14.3±3.2	7.2±2.3	15.7±5.1	

TABLE VIII

Using Method II, the corrected numbers of events, and the ratios $N_{ee}/N_{e\mu}$ and $N_{\mu\mu}/N_{e\mu}$. The numbers are corrected for the purely electromagnetic backgrounds in Table VI and for misidentification losses and triggering efficiencies. They are not corrected for the kinematic cuts in eq. 37. The errors are statistical.

E_{cm} Range (GeV)	3.9-4.3	4.3-4.8	4.8-6.8	6.8-7.4	3.9-4.8	all events
Data Set	2	2	2	2	1	1, 2
$N_{e\mu}$	24±11	8±12	84±25	101±24	46±13	263±40
N_{ee}	3±7	18±11	36±18	64±19	25±10	146±31
$N_{\mu\mu}$	25±9	41±10	46±15	50±16	21±8	183±27
N_{hh}	21±11	1±17	30±23	144±45	17±12	213±56
N_{eh}	39±14	50±18	74±36	1±37	31±16	195±59
$N_{\mu h}$	39±14	50±18	74±36	1±37	31±16	195±59
$N_{ee}/N_{e\mu}$	0.12±.31	4.9±6.3	.43±.24	.64±.24	.54±.27	.56±.14
$N_{\mu\mu}/N_{e\mu}$	1.06±.63	5.9±8.5	.55±.24	.49±.19	.46±.22	.70±.15

TABLE IX

Using Method III, the corrected numbers of events and their ratios. The numbers are corrected for the purely electromagnetic backgrounds in Table VI and for misidentification losses and triggering efficiencies. They are not corrected for the kinematic cuts in eq. 37. The errors are statistical.

E_{cm} Range (GeV)	3.9-4.3	4.3-4.8	4.8-6.8	6.8-7.4	3.9-4.8	all events
Data Set	2	2	2	2	1	1, 2
$N_{e\mu}$	20±12	-11±17	87±28	110±34	46±15	252±51
N_{ee}	2±8	16±24	32±23	66±37	21±12	137±52
$N_{\mu\mu}$	24±12	38±16	52±19	64±23	19±9	197±37
$N_{hh}+N_{hx}+N_{xx}$	38±25	29±41	55±41	183±69	25±18	330±95
$N_{eh}+N_{ex}$	22±18	25±58	47±49	-26±76	35±23	103±111
$N_{\mu h}+N_{\mu x}$	45±27	72±42	70±41	-34±43	24±18	177±80
$N_{ee}/N_{e\mu}$	0.12±.39	--	0.37±.29	0.60±.38	.46±.30	.54±.23
$N_{\mu\mu}/N_{e\mu}$	1.19±.93	--	0.60±.29	0.58±.27	.41±.24	.78±.22

TABLE X

Ratios of corrected numbers of events. The error is statistical.

Method	$N_{ee}/N_{e\mu}$	$N_{\mu\mu}/N_{e\mu}$
I	0.52±.10	0.65±.10
II	0.56±.14	0.70±.15
III	0.54±.23	0.78±.22

TABLE XI

The maximum systematic errors are given. The relative signs indicate the correlation between the effect of the systematic errors on the two ratios, except in the total error. For convenience we have also listed the ratio values and their statistical error from Method II.

	$N_{ee}/N_{e\mu}$	$N_{\mu\mu}/N_{e\mu}$
Systematic error due to background subtractions	± 0.07	± 0.09
Systematic error due to μ loss correction	± 0.06	∓ 0.11
Systematic error due to e loss correction	± 0.08	∓ 0.09
Systematic error due to subtraction of purely electromagnetic background	$+0.10$ -0.15	± 0.08
TOTAL systematic errors if combined in quadrature	$+0.16$ -0.19	± 0.19
Value of ratio with statistical error (one standard deviation) from Method II	0.56 ± 0.14	0.70 ± 0.15

FIGURE CAPTIONS

1. Feynman diagram for production of τ pairs by one-photon exchange.
2. Layout of the SPEAR e^+e^- colliding beams facility. This experiment was carried out in the experimental pit at the bottom of the figure: the west pit.
3. An exploded view of the detector.
4. Feynman diagrams for the two virtual photon process $e^+e^- \to e^+e^-\mu^+\mu^-$.
5. Some Feynman diagrams for the two real photon processes $e^+e^- \to e^+e^-\gamma\gamma$, $e^+e^- \to \mu^+\mu^-\gamma\gamma$.
6. The r distributions for ee, eμ and $\mu\mu$ events for a) all $E_{c.m.}$, b) $E_{c.m.} < 4.8$ GeV c) $E_{c.m.} \geq 4.8$ GeV. To facilitate comparisons the numbers of events in each energy range are normalized so that the area under the eμ data curve is 1.0. The distributions are corrected for hadronic background, but <u>not</u> for the background from the purely electromagnetic processes: ee $\to$ eeee, ee$\mu\mu$, ee$\gamma\gamma$, $\mu\mu\gamma\gamma$. See the text for an explanation of the curves.
7. The cos θ_{coll} distributions for ee, eμ and $\mu\mu$ events for a) $E_{c.m.} <$ 4.8 GeV and b) $E_{c.m.} \geq 4.8$ GeV. To facilitate comparisons the numbers of events in each energy range are normalized so that the area under the eμ data curve is 1.0. The distributions are corrected for the purely electromagnetic processes: ee $\to$ eeee, ee$\mu\mu$, ee$\gamma\gamma$ and $\mu\mu\gamma\gamma$. See the text for an explanation of the stepped lines.

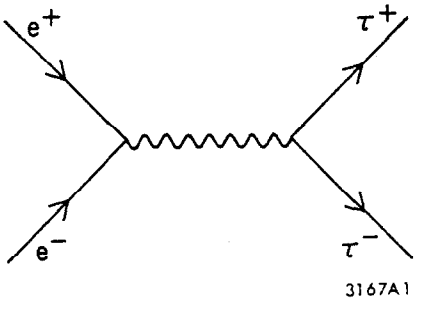

Fig. 1

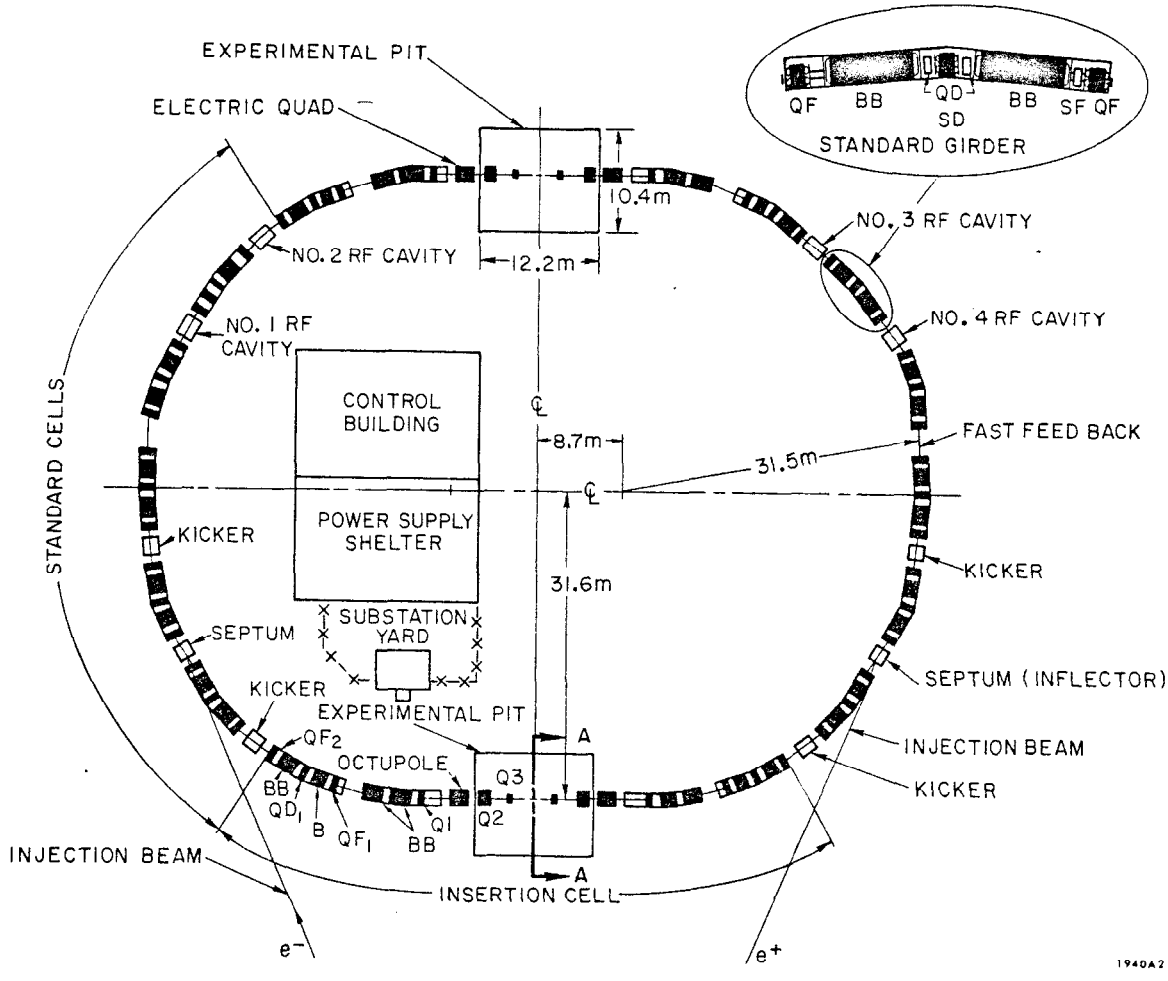
EXPERIMENTAL PIT
ELECTRIC QUAD
QF BB QD SD BB SF QF
STANDARD GIRDER
10.4m
12.2m
NO. 2 RF CAVITY
NO. 3 RF CAVITY
NO. 4 RF CAVITY
NO. 1 RF CAVITY
CONTROL BUILDING
8.7m
31.5m
FAST FEED BACK
STANDARD CELLS
KICKER
POWER SUPPLY SHELTER
31.6m
KICKER
SUBSTATION YARD
SEPTUM
SEPTUM (INFLECTOR)
KICKER
EXPERIMENTAL PIT
QF2
OCTUPOLE
INJECTION BEAM
KICKER
BB
QD1
B
QF1
BB
Q1
Q2
Q3
A
A
INJECTION BEAM
INSERTION CELL
e−
e+
1940A2

Fig. 2

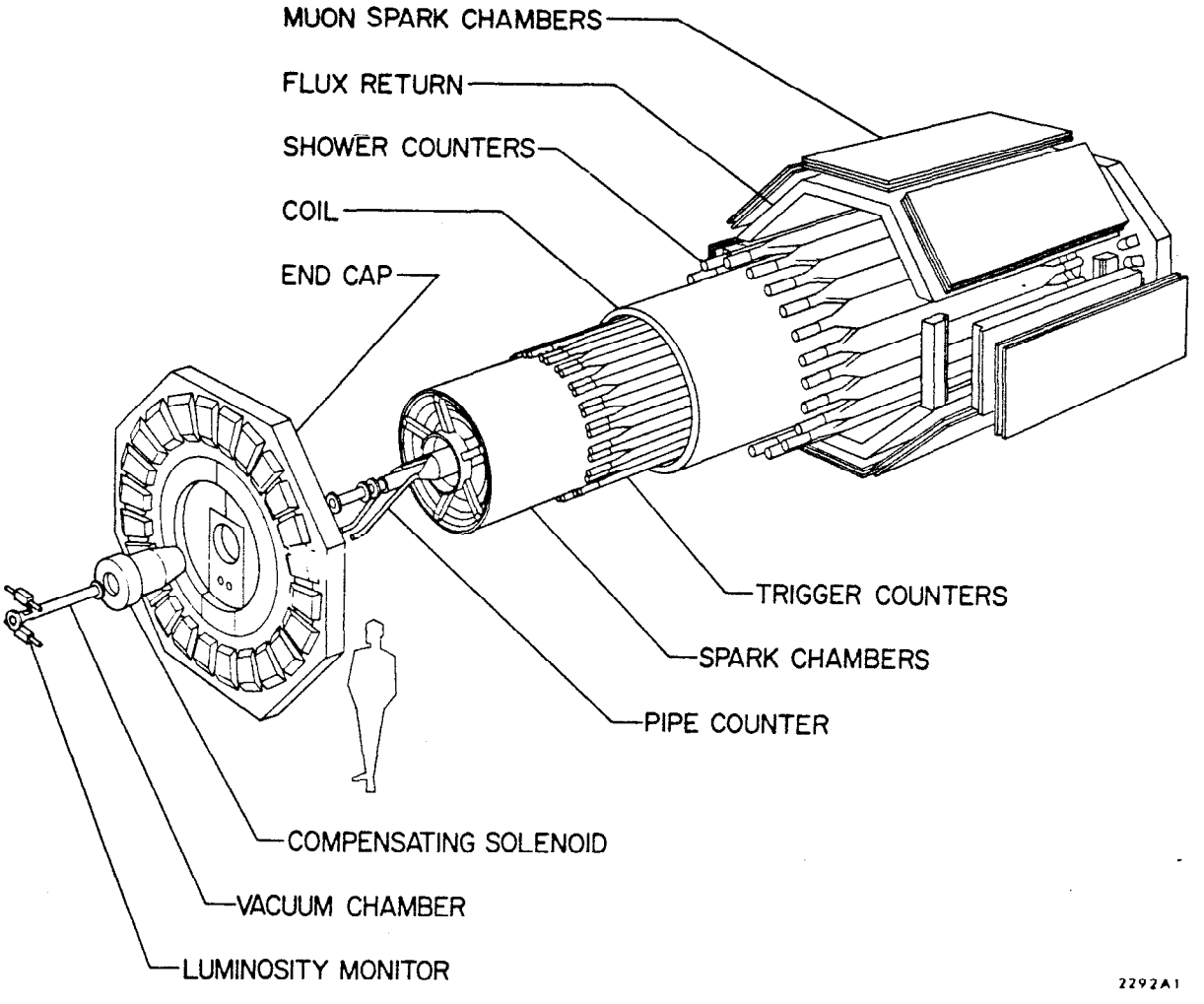
MUON SPARK CHAMBERS
FLUX RETURN
SHOWER COUNTERS
COIL
END CAP
TRIGGER COUNTERS
SPARK CHAMBERS
PIPE COUNTER
COMPENSATING SOLENOID
VACUUM CHAMBER
LUMINOSITY MONITOR
2292A1

Fig. 3

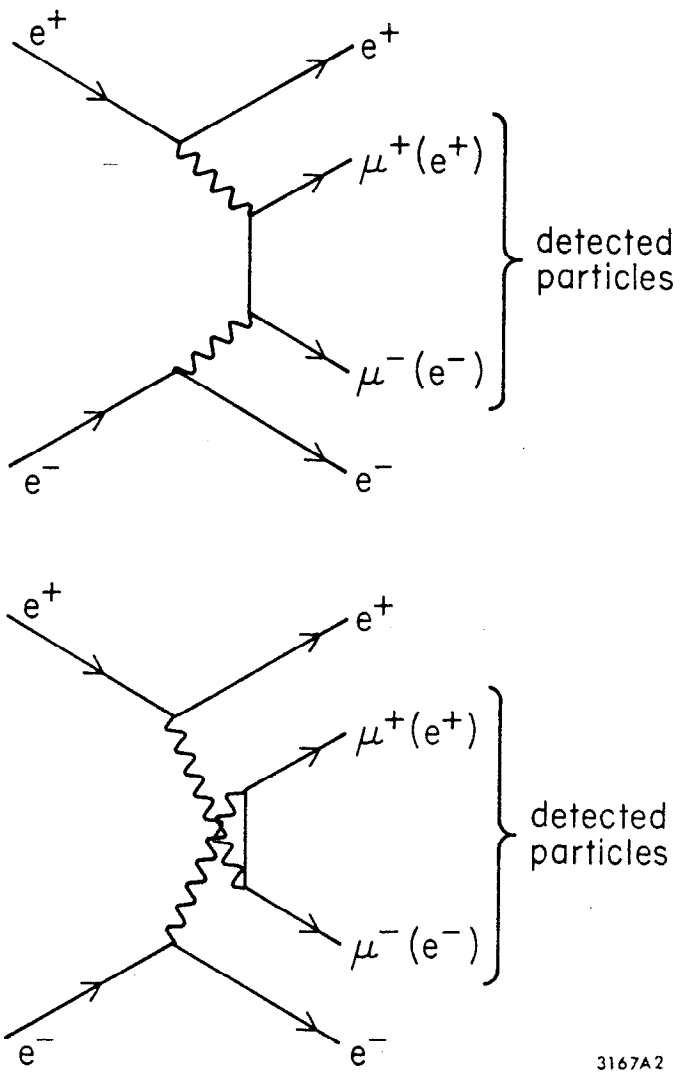
e+
e+
μ+(e+)
detected
particles
μ−(e−)
e−
e−
e+
e+
μ+(e+)
detected
particles
μ−(e−)
e−
e−
3167A2

Fig. 4

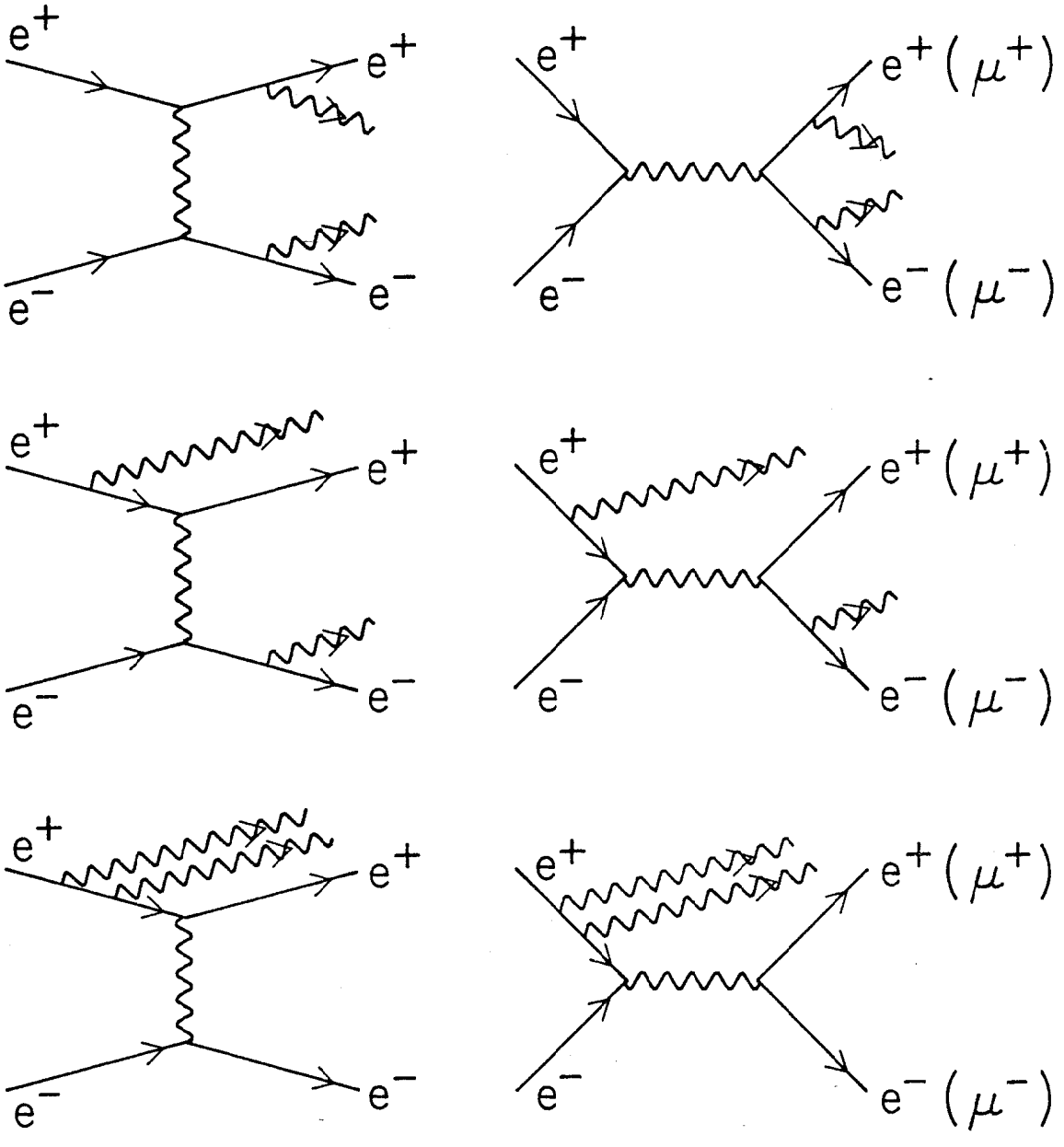

Fig. 5

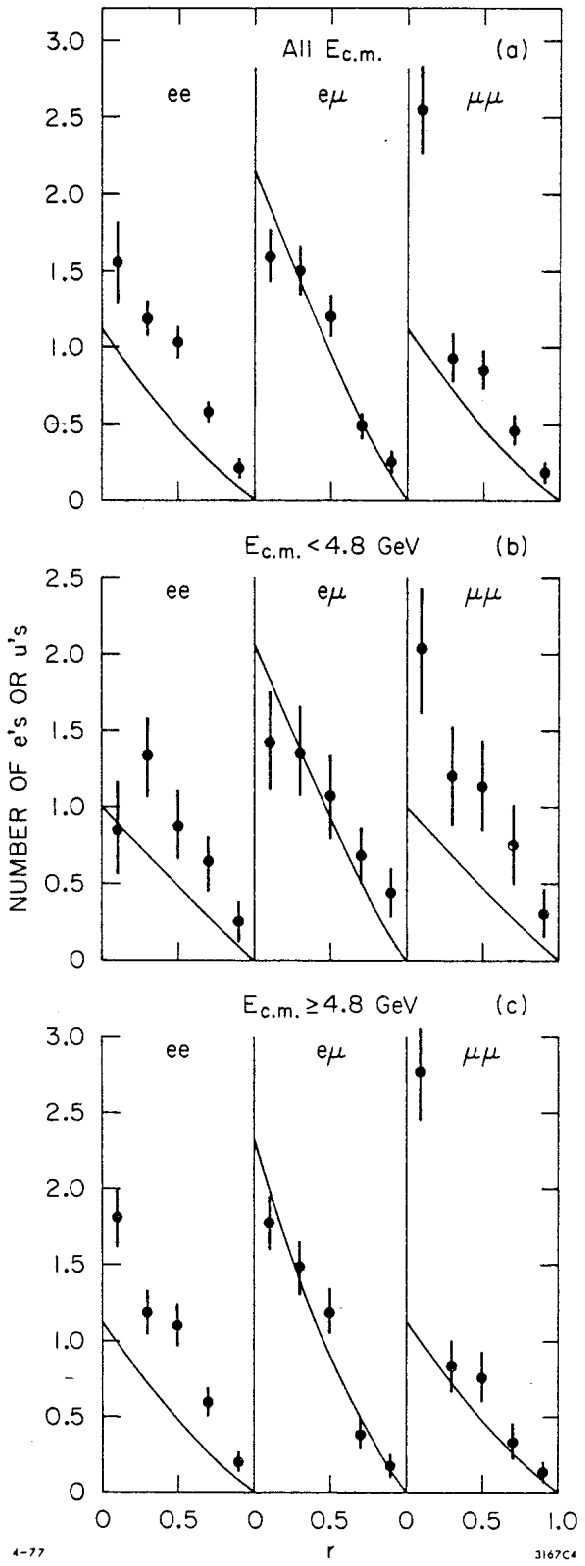
All $E_{c.m.}$
(a)
ee
eμ
μμ
$E_{c.m.}$ < 4.8 GeV
(b)
$E_{c.m.}$ ≥ 4.8 GeV
(c)
NUMBER OF e's OR u's
r
4-77
3167C4

Fig. 6

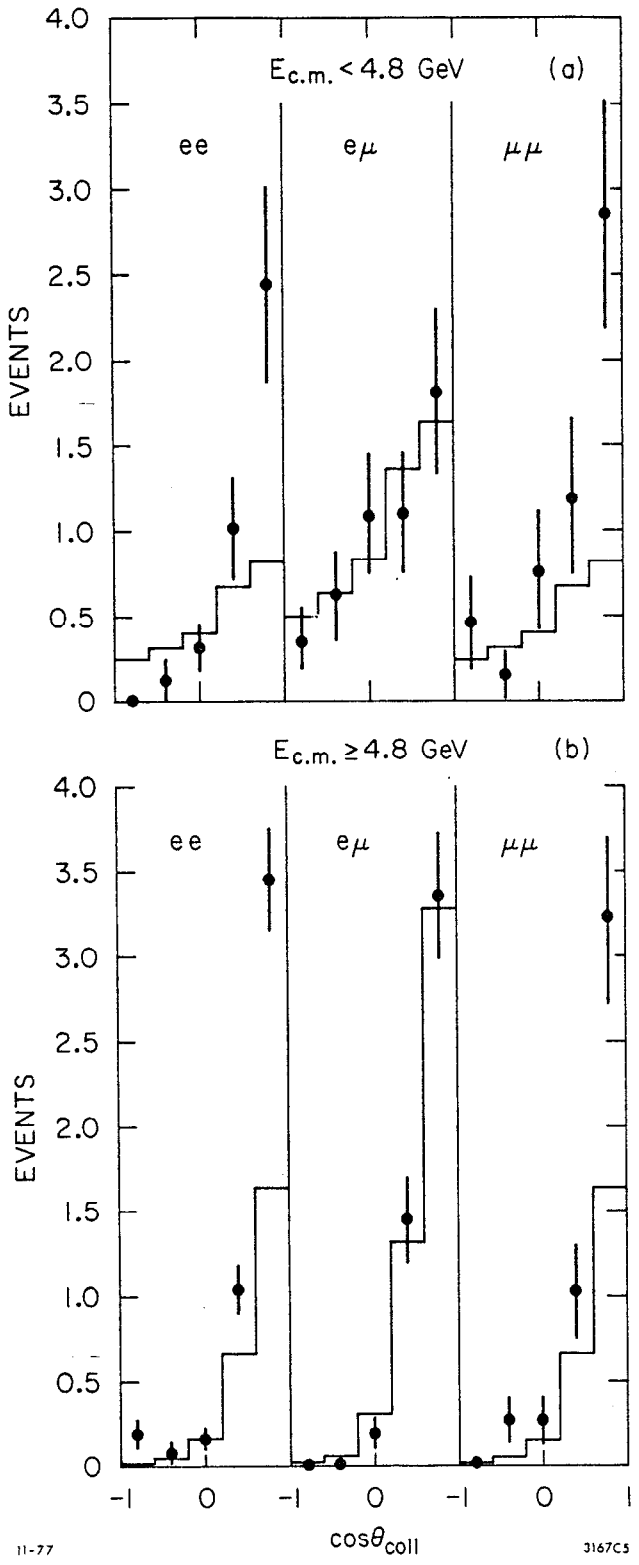
4.0
3.5
3.0
2.5
2.0
1.5
1.0
0.5
0
EVENTS
$E_{c.m.} < 4.8$ GeV
(a)
ee
$e\mu$
$\mu\mu$
$E_{c.m.} \geq 4.8$ GeV
(b)
ee
$e\mu$
$\mu\mu$
EVENTS
-1
0
-1
0
-1
0
1
$\cos\theta_{coll}$
11-77
3167C5

Fig. 7